



Extended Engelund–Hansen type sediment transport relation for mixtures based on the sand-silt-bed Lower Yellow River, China

Kensuke Naito, Hongbo Ma, Jeffrey A. Nittrouer, Yuanfeng Zhang, Baosheng Wu, Yuanjian Wang, Xudong Fu & Gary Parker

To cite this article: Kensuke Naito, Hongbo Ma, Jeffrey A. Nittrouer, Yuanfeng Zhang, Baosheng Wu, Yuanjian Wang, Xudong Fu & Gary Parker (2019): Extended Engelund–Hansen type sediment transport relation for mixtures based on the sand-silt-bed Lower Yellow River, China, Journal of Hydraulic Research, DOI: [10.1080/00221686.2018.1555554](https://doi.org/10.1080/00221686.2018.1555554)

To link to this article: <https://doi.org/10.1080/00221686.2018.1555554>

 View supplementary material 

 Published online: 21 Jan 2019.

 Submit your article to this journal 

 Article views: 80

 View Crossmark data 



Research Paper

Extended Engelund–Hansen type sediment transport relation for mixtures based on the sand-silt-bed Lower Yellow River, China

KENSUKE NAITO  (IAHR Member), PhD Student, *Ven Te Chow Hydrosystems Laboratory, Department of Civil and Environmental Engineering, University of Illinois at Urbana-Champaign, Urbana, IL, USA*
Email: knaito2@illinois.edu (author for correspondence)

HONGBO MA, Postdoctoral Research Associate, *Department of Earth Science, William Marsh Rice University, Houston, TX, USA*
Email: sediment@rice.edu

JEFFREY A. NITTROUER, Assistant Professor, *Department of Earth Science, William Marsh Rice University, Houston, TX, USA*
Email: nittrouer@rice.edu

YUANFENG ZHANG, Professor, *Yellow River Institute of Hydraulic Research, Zhengzhou, Henan, PR China*
Email: zhangdut@hotmail.com

BAOSHENG WU (IAHR Member), Professor, *Department of Hydraulic Engineering, Tsinghua University, Beijing, PR China*
Email: baosheng@tsinghua.edu.cn

YUANJIAN WANG, Deputy Chief Engineer, *Yellow River Institute of Hydraulic Research, Zhengzhou, Henan, PR China*
Email: 576010236@qq.com

XUDONG FU, Professor, *State Key Laboratory of Hydrosience and Engineering, Tsinghua University, Beijing, PR China*
Email: xdfu@tsinghua.edu.cn

GARY PARKER (IAHR Member), Professor, *Ven Te Chow Hydrosystems Laboratory, Department of Civil and Environmental Engineering and Department of Geology, University of Illinois at Urbana-Champaign, Urbana, IL, USA*
Email: parkerg@illinois.edu

ABSTRACT

While the grain-sorting morphodynamics of gravel- and sand-bed rivers has been intensively studied, sand-silt bed rivers such as the Lower Yellow River (LYR), China and the Pilcomayo River, Paraguay/Argentina have received much less attention. As a first step, we use a database from the LYR in the 1980s to develop a grain size specific extended Engelund–Hansen total bed material load relation. We then use this relation in two morphodynamic calculations. First, we “spin-up” the calculation from an arbitrary bed slope over 600 years to reproduce the downstream fining observed before the closing of Xiaolangdi Dam in 2000. We then cut off the sediment supply, and reproduce the observed pattern of bed coarsening as the bed armours in response to degradation. We argue that our model is likely not site-specific, but applies to other sand-silt bed rivers, basic data for which is as yet lacking.

Keywords: Fluvial geomorphology; morphodynamics and channel form; river channels; sediment transport; suspended sediment

1 Introduction

The prediction of sediment transport rates in alluvial rivers is important for many purposes, including sediment and

water resource management (MacArthur, Neill, Hall, Galay, & Shvidchenko, 2008), nutrient management (Cohn, 1995), maintenance of ecological diversity (Allan & Castillo, 2007), short-term/long-term prediction of river morphodynamics

Received 25 September 2017; accepted 23 October 2018/Currently open for discussion.

(Hicks & Gomez, 2016), and design of river disaster countermeasures (MacArthur et al., 2008). A sediment transport relation proposed by Engelund and Hansen (1967) has been recognized as performing well for sand-bed laboratory flumes and sand-bed rivers (Brownlie, 1981; Ma et al., 2017), and is commonly used to predict the total bed material load (i.e. bed load and bed material portion of suspended load). A question arises as to whether the Engelund–Hansen (EH) relation performs well for sand-silt-bed rivers (i.e. rivers in which the silt content of the bed is substantial), such as the Lower Yellow River (LYR, herein defined as the reach between the Xiaolangdi Dam and the river mouth; Fig. 1a) and some of its tributaries, where suspended load is the dominant phase of sediment transport and hyper-concentrated flows (volumetric concentration $> 5\%$, as defined in Pierson, 2005) occasionally occur. Another example of such a river is the Pilcomayo River at the border of Argentina and Paraguay (Martín-Vide, Amarilla, & Zárate, 2014). Wu, van Maren, and Li (2008) addressed this question of applicability of the EH relation to sand-silt-bed rivers based on an analysis on more than 1000 sediment discharge observations from the

Yellow River. They reported that the standard EH relation is a poor predictor of total bed material load in the Yellow River. As discussed in detail below, we also find that the EH relation significantly underpredicts the total load in the LYR (see also Ma et al., 2017). In other words, the LYR has a much higher capacity rate of sediment transport than “typical” sand-bed rivers, for which the EH relation is often used to estimate total bed material load. This difference prevails even after accounting for the much finer characteristic grain size in the LYR as compared to typical sand-bed rivers.

Furthermore, the EH relation is designed to predict the sediment load based only on a single representative bed material grain size. As was recognized by Engelund and Hansen (1967) themselves, the accuracy of the EH relation decreases for widely graded sediment. Local-scale sorting such as armouring and reach-scale sorting such as downstream fining have been recognized as important elements of river morphodynamics (Frings, 2008), especially in gravel-bed rivers and coarse sand-bed rivers, where bedload transport is the dominant phase of sediment transport. In accordance with this observation, a

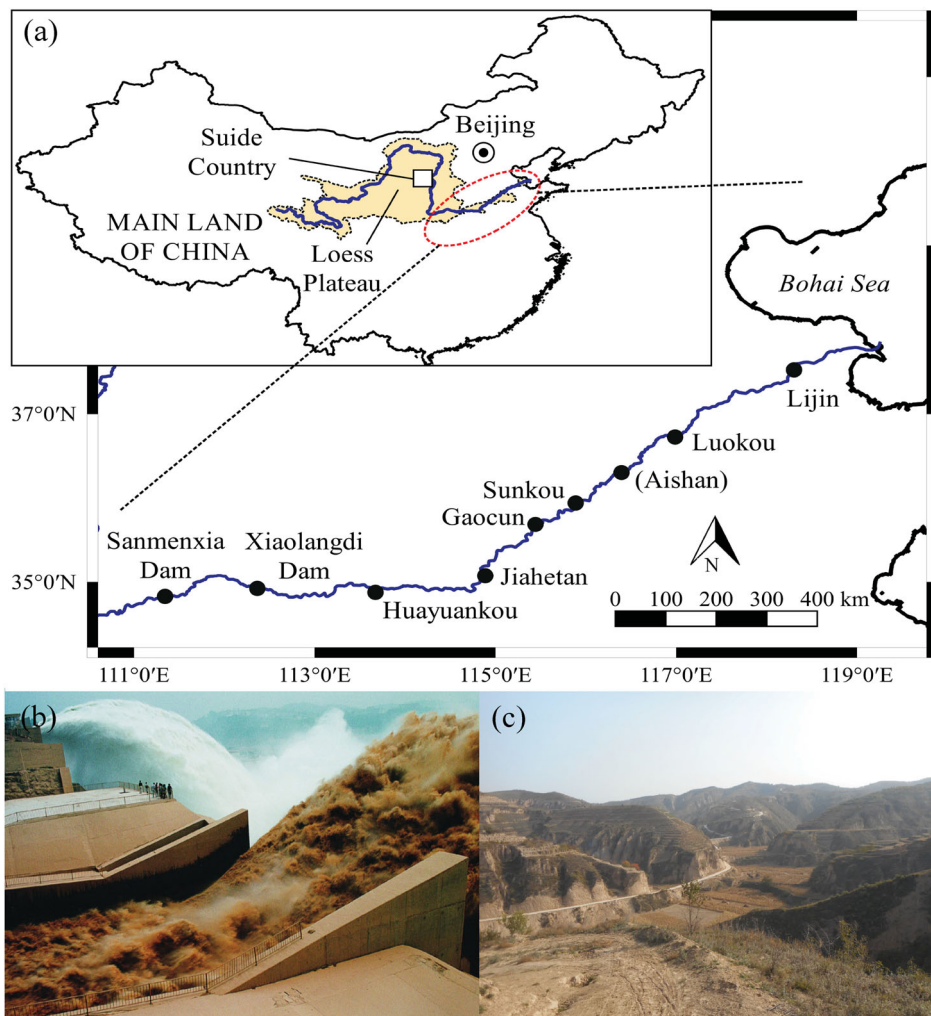


Figure 1 (a) Entire Yellow River basin and the Lower Yellow River, as well as the location of the six major gauging stations and two dams; (b) Loess Plateau in the Suide county (location shown in the map); and (c) sediment sluicing event at the Xiaolangdi Dam (photo courtesy of YRIHR). In (b) the road serves as a scale, and in (c) the people serve as scales

large number of grain size specific sediment transport relations for gravel–sand mixtures and sand mixtures have been developed (e.g. Ashida & Michiue, 1972; Hirano, 1971; Parker, 1990, 1991a, 1991b; Parker & Klingeman, 1982; Wilcock, 1997; Wilcock & Crowe, 2003; Wright & Parker, 2005a, 2005b), and some researchers have developed an extended form of the EH-type relation for mixtures (Blom, Arkesteijn, Chavarrias, & Viparelli, 2017; Blom, Viparelli, & Chavarrias, 2016). However, the application of these relations has been made only to sand-bed and gravel-bed rivers, mostly because grain sorting in sand-silt-bed rivers has not been recognized outside of China.

Sand-silt-bed rivers such as the LYR, however, do exhibit trends of grain sorting. A comprehensive dataset on suspended sediment load and its grain size distribution (GSD), as well as bed material GSD, was assembled in the period 1980–1990 by the Yellow River Institute of Hydraulic Research (YRIHR), China (Long & Zhang, 2002; Zhang, Long, & Shen, 1998). These data show a clear trend toward downstream fining of the bed material (Fig. 2). This pattern of downstream fining, which predates the closing of Xiaolangdi Dam in 2000, appears to be a natural response as the river debouches from the relatively high-slope Loess Plateau to the relatively low-slope North China Plain. Moreover, provided that the particles that compose the bed surface of the LYR are primarily silt and sand, it is reasonable to consider that the downstream fining is dominated by size-selective transport rather than abrasion of the particles (Parker, 1991a). Figure 2 further demonstrates that the LYR has shown significant bed degradation and coarsening since the closure of Xiaolangdi Dam (Chen, Zhou, & Qiang, 2012; Ta, Wang, & Jia, 2011). This is a response to the dramatic reduction of the sediment supply to the LYR due to the installation of Xiaolangdi Dam. The pattern of coarsening has been gradually propagating downstream since 2000.

In order to reproduce the pattern of downstream variation of grain size in the LYR, as well as compute the time evolution

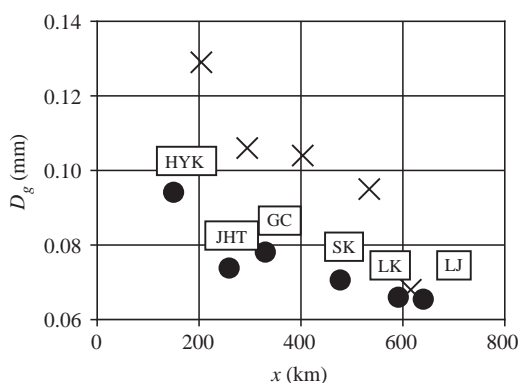


Figure 2 Downstream variation of D_g . Black dots are from the dataset collected in the period 1980–1990 which has been used in this study, and crosses are the dataset collected in 2009 and reported by Chen et al. (2012). The single point at Jiahetan notwithstanding, the data show a clear overall trend toward downstream fining. HYK, JHT, GC, SK, LK and LJ stand for Huayuankou, Jiahetan, Gaocun, Sunkou, Loukou and Lijin, respectively

of this pattern, it is necessary to have a grain size specific sediment transport relation. A knowledge of sorting in the lower reach of a sand-bed river, where the river flows into a standing body of water such as the ocean, can provide insight into the understanding of the dynamics of delta evolution. For example, a grain size specific sediment transport relation allows prediction of the range of sediment sizes that is available for delta construction and delivery to the sea. Most sediment transport relations designed for the Yellow River are based on a single characteristic grain size of the bed, or of the suspended load (e.g. Wu & Long, 1993; Yang, Molinas, & Wu, 1996; Zhang, 1959). Zhang, Huang, and Zhao (2001; as reported in He, Duan, Wang, & Fu, 2012) present a sediment transport relation designed for the Yellow River that does indeed calculate grain size specific transport rates. This formulation, however, calculates the volume fraction content in the load as an algebraic function of the volume fraction content in the bed, and is thus in conflict with the grain size specific Exner equation of sediment continuity.

In this study, we present a surface-based grain size specific sediment transport relation as an extension of the generalized EH-type relation using a single grain size that was recently proposed by Ma et al. (2017). Our relation is developed so as to allow calibration using site-specific field data. Therefore, the model is applicable to both sand-bed rivers and sand-silt-bed rivers. Here we evaluate the formulation using data for the LYR. We use the relation to predict “broad-brush” aspects of long-term morphodynamics such as the evolution of the river bed profile and GSD of the bed surface in the LYR.

2 The LYR and dataset

The Yellow River is a silt-rich river that carries a large amount of fine sediment in suspension at relatively high concentrations, i.e. up to hundreds of kilograms per cubic metre (Jiongxin, 1999). It has been recognized as the second largest in the world in terms of the sediment load delivered to the ocean (Milliman & Meade, 1983). The river originates in the Bayankala Mountains and flows through the Loess Plateau, which is located along the middle reach of the Yellow River and where about 90% of the sediment load is produced (Wang et al., 2016; Yu, Shi et al., 2013; Yu, Wang et al., 2013). Until the closure of Xiaolangdi Dam in 2000, the annual sediment load of the LYR was as high as 1.08 Gt, accounting for 6% of the total sediment flux from global rivers to the ocean (Milliman & Meade, 1983). Due to this high sediment load, the river system had until recently been aggrading at a high rate. In the lower reach, the bed elevation is higher by up to 10 m than the surrounding floodplain (“hanging riverbed”, Fig. S2b in the online supplemental data). This high sediment load has also led to the rapid formation of a new delta lobe, which began prograding in 1855 and was more than 5000 km² in area in 2010 (Wang et al., 2010). As described below, since the closure of Xiaolangdi Dam, however, the sediment load in the LYR has dropped substantially.

Xiaolangdi Dam was installed about 860 km upstream of the river mouth and closed in 2000. It is located near where the river debouches from the Loess Plateau to the North China Plain. Once per year, during the flood season (July–October), water and sediment are released from Xiaolangdi Dam in order to preserve reservoir capacity and scour the bed of the river downstream (Ma et al., 2017; Yu, Wang et al., 2013). It is intended that this scouring will mitigate flood risk. Wang et al. (2007) pointed out that the installation of large dams such as Xiaolangdi Dam and Sanmenxia Dam, which is located about 130 km upstream of Xiaolangdi Dam, as well as climate change, have brought about a step-wise decrease in the water and sediment discharge to the lower reach and the Bohai Sea. Figure 1a shows the Yellow River, two major dams, i.e. Xiaolangdi Dam and Sanmenxia Dam, and six major hydraulic gauging stations. A modern view of the Loess Plateau in Suide County, Shaanxi Province is shown in Fig. 1b. It should be mentioned that the land surface in parts of the Loess Plateau is presently relatively more vegetated than in the recent past, owing to vigorous efforts toward revegetation associated with the “Grain to Green Program” launched in 1999 (Chen et al., 2015). Figure 1c shows a sediment sluicing event at Xiaolangdi Dam. In this study, we focus on the lower part of the Yellow River, i.e. the LYR.

Datasets used in this paper were developed in 1980–1990 by the Yellow River Institute of Hydraulic Research, Zhengzhou, China, at the following six major gauging stations along the LYR in order downstream; Huayuankou, Jiahetan, Gaocun, Sunkou, Luokou and Lijin (Long & Zhang, 2002; Zhang et al., 1998, Fig. 1a). Each dataset contains records of flow rate, bed slope, flow width, flow depth, mass concentration of suspended sediment, and GSD of both bed material and suspended load, all at what was interpreted to be quasi-equilibrium state, in which deposition and entrainment of the bed material are locally not far out of balance. It is worth repeating that the datasets were developed before the construction of Xiaolangdi Dam, which was closed in 2000. It should also be noted that the dataset on sediment transport of the LYR does not report direct measurements of bed load; only the suspended load was directly measured. The bedload transport rate was estimated according to the procedure discussed in Ma et al. (2017); it was found to be negligible compared to the suspended load.

3 Generalized Engelund–Hansen formula (the EH relation) for single grain size

Figure 3 shows the GSDs of bed material and suspended load at the Lijin gauging station. The GSDs of bed material and suspended load of the Mississippi River at St. Louis, USA, which is considered as a typical sand-bed river, are also plotted for comparison. It is seen that the bed of the LYR contains a large fraction of silty sediment that is finer than 62 μm , a range that is typically considered to be wash load in most sand-bed rivers (e.g. Woo, Julien, & Richardson, 1986), such as the Mississippi

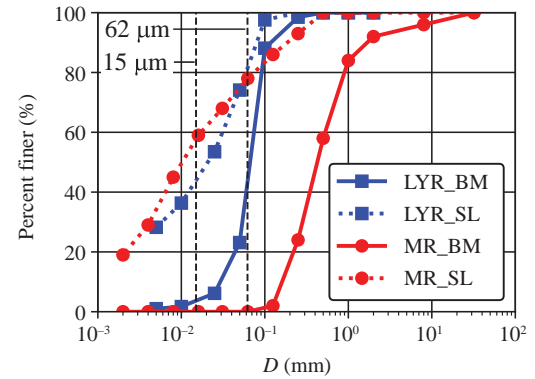


Figure 3 GSD of the bed material and suspended load of the LYR at Lijin (LYR_BM and LYR_SL, where BM indicates bed material and SL indicates suspended load) averaged over the period 1980–1990; and GSD of the Mississippi River at St. Louis, USA (MR_BM and MR_SL) averaged over the period 1960–2011. Included in the plot are vertical lines denoting 62 μm , corresponding to a “standard” divider for bed material load versus wash load, and 15 μm , the divider used herein for the LYR

River, as can be seen in Fig. 3. Wash load is defined as the sediment that is being transported, but is too fine to be found in easily measurable quantities in the bed (Bettes, 1994). For the LYR, we select 15 μm (0.015 mm) to be the cut-off size for wash load (Ma et al., 2017). Sediment finer than 15 μm is considered to be wash load, and hence is excluded in the development of the sediment transport relation herein.

A generalized form of the total load relation in accordance with the EH relation takes the form:

$$C_f q_T^* = A(\tau_g^*)^B \quad (1)$$

where C_f is the bed friction coefficient, q_T^* is the Einstein number or dimensionless total load per unit width, and τ_g^* is Shields number or dimensionless bed shear stress based on bed geometric mean grain size D_g . The parameters A and B are constants, with $A = 0.05$ and $B = 2.5$ for the original EH relation. In the above relation, the friction coefficient C_f is defined as:

$$C_f = \frac{\tau_b}{\rho U^2} \quad (2)$$

where τ_b denotes bed shear stress, U denotes depth-averaged flow velocity, and ρ denotes the density of the water–sediment mixture. The Einstein number q_T^* is defined as:

$$q_T^* = \frac{q_T}{\sqrt{RgD_g^3}} \quad (3)$$

in which q_T is total bed material load per unit width, R is submerged specific gravity of sediment ($R = 1.65$ for quartz), and g is gravitational acceleration. While the original EH relation makes use of the median grain size of the bed surface D_{50} , we instead make use of geometric mean grain size D_g in a preliminary treatment of sediment mixtures. Assuming that the

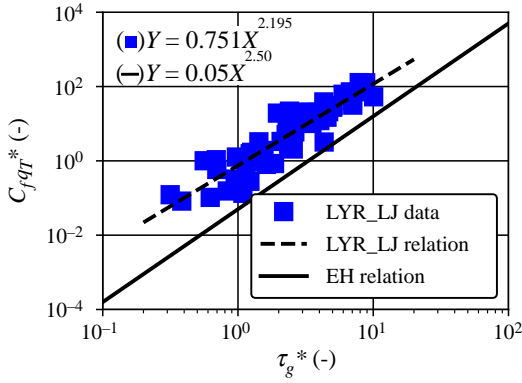


Figure 4 Plot of observed data of $C_f q_T^*$ versus τ_g^* for the LYR at Lijin (LYR_LJ data), along with a fit line for our EH type relation adapted for the LYR (LYR_LJ relation) and for the original EH relation (EH relation)

flow is steady and uniform (i.e. normal flow approximation), the Shields number τ_g^* is computed as:

$$\tau_g^* = \frac{\tau_b}{\rho R g D_g} = \frac{HS}{RD_g} \quad (4)$$

where H and S denote flow depth and downstream channel slope, respectively. Implicit in Eq. (4) is the evaluation of the bed shear stress τ_b from the form appropriate for equilibrium (normal) flow:

$$\tau_b = \rho g HS \quad (5)$$

This assumption is justified for the quasi-equilibrium case used for the LYR data, as outlined in Ma et al. (2017).

Figure 4 shows a plot of the product of the dimensionless friction coefficient and the Einstein number, i.e. $C_f q_T^*$, versus Shields number τ_g^* , along with the data from the Lijin gauging station and the best fit of the generalized EH relation (Eq. (1)). A linear regression analysis indicates that the coefficient A and exponent B in Eq. (1) for the Lijin dataset are $A = 0.751$ and $B = 2.195$, with a value of the coefficient of determination $R^2 = 0.85$. It is seen that the original EH relation greatly underestimates the total load, indeed by a factor of nearly 20. This indicates that the original EH relation is not appropriate for the case of sand-silt-bed rivers with high sediment loads such as the LYR.

4 Surface-based grain size specific sediment transport relation

Parker (1990) proposed a grain size specific bed load transport relation, assuming that the bed is classified into two layers: surface layer (or active layer) and subsurface layer (or substrate). The relation is a “surface-based” relation, since it requires knowledge of the GSD of the bed surface, as opposed to a “subsurface-based” relation that requires the knowledge of the subsurface of the bed (Parker, 1990). Although the GSD of

sediment yield of the reach may in some cases be similar to that of the subsurface, it is the exposed sediment at the bed surface that is directly available for entrainment into transport from the bed (Parker, 1990).

Adapting the form of Parker (1990) to correspond with EH, we define the general dimensionless form of the grain size specific bed material load as follows:

$$N_i^* = \frac{C_f R g q_T f_i}{u_*^3 F_i} \quad (i = 1, 2, 3, \dots, N) \quad (6)$$

where N_i^* is dimensionless bed material transport rate for the grain in i th size range, f_i is the volume fraction content of the i th size range grain in the total bed material load, F_i is the volume fraction content of the i th grain size range in the bed surface (active layer), and u_* is the shear velocity. Here we relate the above parameters to hydraulic conditions using power functions as follows, so as to parallel the original form of the EH relation:

$$N_i^* = A_i (\tau_i^*)^{B_i} \quad (7)$$

where A_i and B_i are coefficients and exponents for the i th grain size range. In the case of the original EH relation, designed for a single grain size, A and B are 0.05 and 1, respectively. Also τ_i^* is the Shields number for the i th size range, defined by means of Eq. (4) as:

$$\tau_i^* = \frac{HS}{RD_i} = \tau_g^* \frac{D_g}{D_i} \quad (8)$$

Here D_i denotes the characteristic bed material size of the i th grain size range. Therefore, one can rewrite Eq. (7) as:

$$N_i^* = A_i \left(\tau_g^* \frac{D_g}{D_i} \right)^{B_i} \quad (9)$$

It should be noted that unlike other surface-based relations such as the ones by Parker (1990), Tsujimoto (1991), and Hunziker and Jaeggi (2002), there is no critical Shields number or reference Shields number in the present formulation. This is because the flow is considered to be always well above the threshold condition for sediment entrainment for any grain size on the bed surface, allowing neglect of the effect of critical Shields number. Parker (1990) and Kuhnle (1992) have indicated that coefficients similar to A_i and B_i can be cast as functions of grain size D_i . We thus empirically relate A_i and B_i to the corresponding grain size of the i th range and geometric mean grain size as follows:

$$A_i = f_A \left(\frac{D_i}{D_g} \right), \quad B_i = f_B \left(\frac{D_i}{D_g} \right) \quad (10)$$

The dimensionless form of the total bed material load N_T^* is expressed in the form of the summation below:

$$N_T^* = \frac{C_f R g q_T}{u_*^3} = \sum_{i=1} \left[F_i A_i \left(\tau_g^* \frac{D_g}{D_i} \right)^{B_i} \right] \quad (11)$$

The advantage of the form of the above equation is that the effect of grain size is placed only on the right-hand side, so limiting spurious correlation in grain size when determining the regressions. Moreover, in terms of sediment sizes, this relation requires only the GSD of the bed material. It does not require knowledge concerning the size of sediments that are in transport in order to estimate the bed material load transport rate. This is in contrast to e.g. the relations of Zhang (1959), Wu and Long (1993) and Yang et al. (1996), which are inherently circular in requiring advance knowledge of parameters pertaining to the load in order to compute it. The bed material transport rate of sediment in the i th grain size range q_i and total bed material transport rate q_T are respectively given as:

$$q_i = q_T f_i = F_i \frac{u_*^3}{C_f R g} [A_i (\tau_i^*)^{B_i}] \quad (12)$$

$$q_T = \sum_{i=1} q_i = \frac{u_*^3}{C_f R g} \sum_{i=1} \left[F_i A_i \left(\tau_g^* \frac{D_g}{D_i} \right)^{B_i} \right] \quad (13)$$

It should be pointed out that in the present formulation, if a GSD is not represented in the bed surface, it will not be represented in the bed material transport as well. Size ranges that are present in suspension, but not present above some threshold in the bed (here we use 5%, as documented in Ma et al., 2017), are categorized as wash load. The volume fraction content of the i th grain size in the total bed material load f_i is computed as follows:

$$f_i = \frac{F_i A_i \left(\tau_g^* \frac{D_g}{D_i} \right)^{B_i}}{\sum \left[F_i A_i \left(\tau_g^* \frac{D_g}{D_i} \right)^{B_i} \right]} \quad (14)$$

5 Implementation

5.1 Model implementation for the case of the LYR

We implement the relation for the case of the LYR with the use of the Lijin dataset. Here the GSD is divided into five bins ($N = 5$): $D_i = 0.019, 0.035, 0.071, 0.158$ and 0.354 mm. In treating such fine material, it should be recognized that cohesiveness can play a significant role in sediment transport. In the case of the Yellow River, however, cohesiveness is rather weak (Tian, Wang, Li, & Li, 2016; Wang, Wang, & Tian, 2007). In this analysis, therefore, we do not consider the effect of sediment cohesion.

Plots of N_i^* versus τ_i^* are made so as to obtain the values of A_i and B_i empirically using least-square linear regression analysis for each grain size range (Fig. 5). The values of τ_i^* are calculated from the measured data by means of Eq. (8), and the single representative value of $67 \mu\text{m}$ for D_g . Table 1 summarizes the values of A_i and B_i , as well as the coefficient of determination R^2 and standard error μ for each grain size range

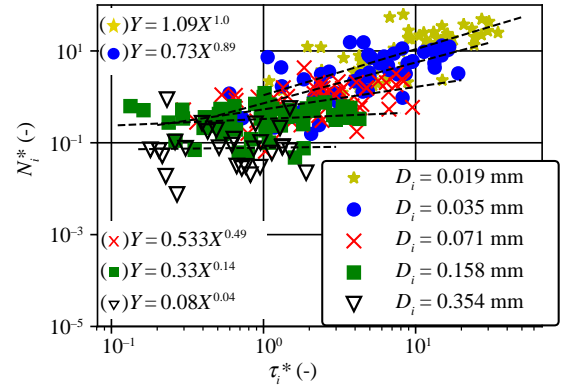


Figure 5 Plot of N_i^* versus τ_i^* . It is seen that dependency of N_i^* on τ_i^* decreases with increasing grain size. The results of the regression analysis are also summarized in Table 1

Table 1 Results of linear regression analysis used to find the values of A_i and B_i

	D_i (mm)				
Parameters	0.019	0.035	0.071	0.158	0.354
A_i	1.09	0.72	0.53	0.33	0.08
B_i	1.00	0.89	0.49	0.14	0.04
R^2	0.48	0.40	0.21	0.03	0.01
μ	0.38	0.39	0.34	0.31	0.46

The coefficient of determination R^2 and the standard error μ are also shown. The regression analysis is shown in Fig. 5.

obtained from the analysis. Regression results indicate that the correlation is not significant in a statistical sense, especially for coarser grain sizes. This is likely due to the inherent scatter in the data associated with a river with high variability such as the Yellow River. This limitation notwithstanding, the correlations are readily apparent by eye, and in the absence of alternative data, we use them as a practical basis for a method to compute the transport of mixed sizes in the Yellow River. It is seen in Table 1 that the values of both A_i and B_i decrease with increasing grain size D_i . This suggests that the transport rate of relatively coarser grains is less dependent on the flow rate than that of the relatively finer grains. This contrasts with the finding by Kuhnle (1992), in which it was found that B_i slightly increases with increasing D_i/D_g (Blom et al., 2017).

We now relate the values of A_i and B_i so obtained to the corresponding grain size D_i normalized by the bed surface geometric mean grain size D_g (Fig. 6), in order to obtain a predictive relation for A_i and B_i . Regression analysis yields the following relations for A_i and B_i for given grain size:

$$A_i = 0.455 \left(\frac{D_i}{D_g} \right)^{-0.839} \quad (15)$$

$$B_i = 0.353 \left(\frac{D_i}{D_g} \right)^{-1.157} \quad (16)$$

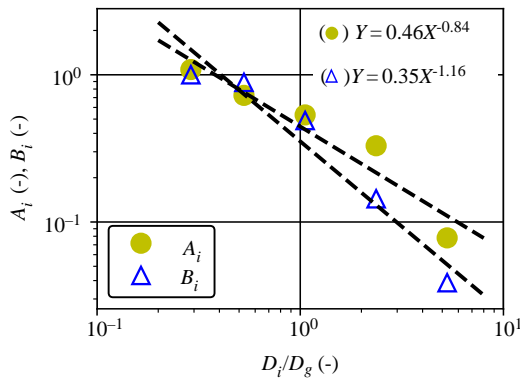


Figure 6 Plot of A_i and B_i in Eq. (9) versus D_i/D_g . Values of A_i and B_i both decrease with increasing grain size

Lastly, we illustrate the applicability of the proposed relation, which was obtained using data at the Lijin gauging station, with the use of the datasets at the Gaocun and Sunkou stations, i.e. the two nearest stations upstream. Figure S1 in the online supplemental data shows a comparison of the proposed relation against the observed data at Gaocun and Sunkou stations. The plot is made in the form of a generalized EH relation ($C_f q_T^*$), rather than the proposed form for the total bed material load using the parameter N_T^* . It is seen in Fig. S1 that while

the proposed relation developed based upon Lijin dataset does not necessarily represent the entire LYR accurately, it shows a general pattern of agreement between predicted and measured values. The development of a site-specific relation applicable to each gauging station may be needed for more precise prediction of the sediment bed material transport rate. The methodology for this is straightforward but is not implemented in this first analysis. Ma et al. (2017), for example, have shown that the coefficient A and exponent B in Eq. (1) for total load vary mildly but systematically in the streamwise direction. These comments notwithstanding, our relation is adequate for a “broad-brush” treatment of the morphodynamics of the LYR as a whole.

5.2 General behaviour of the implemented model

Figure 7 shows the general behaviour of the proposed sediment mixture transport relation, as implemented for a case based on parameters for the LYR. The bed shear stress τ_g^* is computed for fixed values of channel slope, channel resistance and channel width, and over a range of values for water discharge. More specifically, down-channel slope is 0.00015, dimensionless Chezy resistance coefficient is 30, channel width is 500 m, and water discharge varies from 100 to 10000 $\text{m}^3 \text{s}^{-1}$. With the

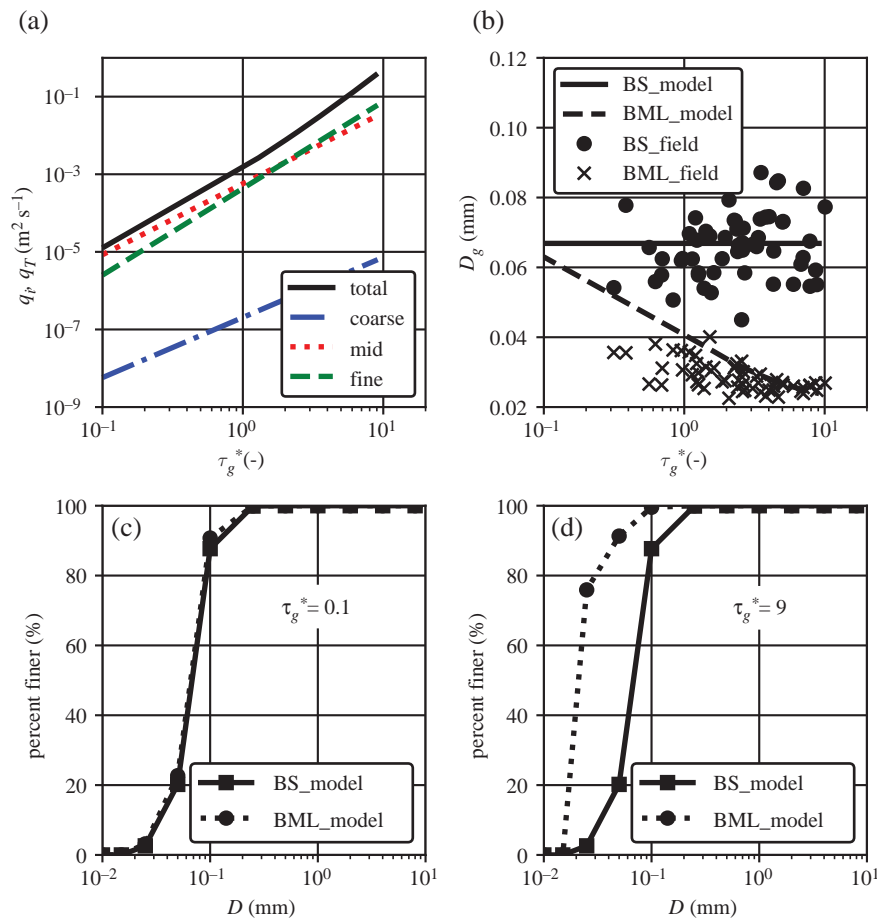


Figure 7 Illustration of general behaviour of the proposed bed material transport model. (a) Relation between q_T , as well as q_i (coarse, mid, and fine) and τ_g^* . (b) Geometric mean grain size of total bed material load (dashed line (BML_model): model results, crosses: observed data) and bed surface (solid line (BS_model): model results, dots: observed data) versus τ_g^* . (c) GSD of bed surface (BML_model) and bed material load (BML_model) for the case $\tau_g^* = 0.1$. (d) Corresponding distribution for the case $\tau_g^* = 9$

use of the bed material GSD at the Lijin gauging station, total bed material load, as well as bed material load for each grain size range is computed over a range of values of bed shear stress τ_g^* corresponding to varying water discharge. Figure 7a shows the total bed material load q_T , as well as the bed material load for the three grain size ranges with characteristic sizes 0.354 mm (coarse), 0.158 mm (middle), and 0.035 mm (fine). It is seen that both total bed material load q_T and the bed material load for each grain size range q_i increase with increasing bed shear stress τ_g^* . Unlike gravel bed rivers where the GSD of the bed material load approaches that of the bed surface as the bed shear stress increases (Parker, 2008), in the case of the LYR the GSD of the load diverges from that of bed material and becomes finer as the bed shear stress increases (Fig. 7b). This fining of the load is associated with the negative correlation of the exponent B_i with D_i/D_g seen in Fig. 6 (Eq. (16)). Figure 7c and 7d show the GSDs of the bed material and the load for low bed shear stress ($\tau_g^* = 0.1$) and high bed shear stress ($\tau_g^* = 9$), respectively, for a set bed slope of 0.00015. Figure 7 also demonstrates that the fraction of fine material increases with increasing bed shear stress, causing overall fining of the bed material load.

The relation for suspended load of Wright and Parker (2004) in sand-bed rivers also does not satisfy equal mobility at high shear stress. Instead, it satisfies “equal entrainability”, whereby the entrainment rate into suspension is linearly proportional to fraction content in the bed surface layer. The suspended transport rate of each grain size range is then calculated using a stratification-corrected Rousean formulation. The exponent in this formulation includes the ratio u_*/v_{si} : this guarantees a bias toward a suspended load that is finer than the bed surface. It should be noted that whereas in our illustrative calculation for the Yellow River the GSD of the bed surface is fixed, the morphodynamics calculations presented in the following section allow the bed surface sediment composition to change as the channel bed evolves.

6 Calculational example: downstream fining, bed coarsening and 1-D morphodynamics calculation of the LYR

After the latest major avulsion of the river in 1855 (e.g. Wright et al., 1990; Xue, 1993), the channel bed of the LYR continuously aggraded due to the high sediment load until the river bed near Huayuankou was about 10 m higher than the surrounding floodplain beyond the levees (Wu, Wang, Xia, Fu, & Zhang, 2008). This aggradation was brought to a halt by the closure of Xiaolangdi Dam, 120 km upstream of Huayuankou, in 2000. We refer to the bed in the two decades before the closure of this dam as in the “pre-Xiaolangdi” condition. Since most of the bed material that now flows into Xiaolangdi Dam is captured by the dam (“post-Xiaolangdi” condition), the bed material supply to the LYR has been substantially reduced, leading to degradation of the bed and coarsening of the bed surface (e.g. Chen et al.,

2012; Yu, Shi et al., 2013; Yu, Wang et al., 2013). Moreover, as mentioned above, datasets for the LYR indicate a trend toward downstream fining both before and after the installation of Xiaolangdi Dam (Chen et al., 2012; see also Fig. 2). Here, with the use of our proposed grain size specific total load relation, we study the long-term evolution of the GSD of the bed surface, as well as the bed elevation profile. Our purpose is to demonstrate the use of our proposed sediment transport relation and its capability for predicting the general patterns of downstream fining, as well as the bed coarsening induced by bed material supply reduction, that have been observed in the LYR. This simulation is not intended to precisely reproduce current conditions of the LYR. In order to do this, it would be necessary to include a plethora of elements of geometric complexity (e.g. multiple levees of spatially varying height and width and detailed hydrographs; He et al., 2012) that would distract from the purpose of this paper.

6.1 Modelling formulation

Wright and Parker (2004) and He et al. (2012) use an entrainment-based formulation for the Exner equation of sediment continuity. That is, they calculate the variation in bed elevation and surface GSD in terms of the difference between an entrainment rate into suspension and a deposition rate from suspension. Here, however, we use a flux-based formulation, in which the local sediment transport rate equals the capacity value for the flow, and the bed elevation variation is related to the downstream gradient in streamwise sediment transport rate. The use of the flux form is likely generally appropriate because the LYR dataset was developed under quasi-equilibrium conditions, in which the flow carries bed material at its transport capacity and sediment deposition to the bed and sediment entrainment of the sediment from the bed are locally in balance (Long & Zhang, 2002; Zhang et al., 1998).

As shown in Fig. S2a in the online supplemental data, we consider a reach of the LYR in which the channel is sinuous within a floodplain. The channel has sinuosity Ω . The modelling equations are composed mainly of three equations: a momentum equation for the flow, a sediment transport relation, and sediment mass conservation equation. The flow is assumed to be steady and uniform, i.e. we use the normal flow approximation. This yields the following form of the momentum balance equation:

$$Q_{bf} = Cz\sqrt{gH_{bf}}SH_{bf}B_{bf} \quad (17)$$

where Q_{bf} is bankfull discharge, Cz is dimensionless Chezy resistance coefficient, H_{bf} is bankfull depth, and B_{bf} is bankfull width. In order to simplify the simulation of long-term morphodynamics, we assume that the river is at bankfull conditions, which are sustained for the morphodynamically active time fraction I_f (flood intermittency factor, Paola, Heller, & Angevine, 1992). That is, the river is assumed to be at low flow and inactive for time fraction $1 - I_f$. For the sediment transport relation,

we employ our proposed grain size specific total load relation, i.e. Eqs (12) and (13). For bed material mass conservation, we employ the active layer concept first proposed by Hirano (1971). The active layer is the surface layer of the bed which directly interacts with bed material load via exchange of mass, whereas the substrate is the layer that interacts only with the active layer via aggradation or degradation (Fig. S3 in the online supplemental data). The active layer is, by definition, assumed here to have no vertical structure in terms of GSD. We implement the standard 1-D Exner equation in such a way that the equation is capable of accounting for multiple grain sizes using the active layer concept as follows:

$$(1 - \lambda_p) \left[F_{li} \frac{\partial(\eta - L_a)}{\partial t} + \frac{\partial(F_i L_a)}{\partial t} \right] = - \frac{(1 + \Lambda) \Omega I_f B_{bf}}{B_f} \frac{\partial(q_T f_i)}{\partial x} \quad (18)$$

where t is time, x is the streamwise coordinate, F_{li} is the fraction in i th grain size at the interface between the substrate and the active layer, L_a is active layer thickness, F_i is the volume fraction content of i th grain size range in the active layer, λ_p is bed porosity, and B_f is floodplain width (Figs S2 and S3 in the online supplemental data). In addition, Λ is volume fraction of wash load deposited on the floodplain per unit deposition of bed material load. That is, we assume that for each unit of bed material deposition, Λ units of wash load are deposited so as to construct the channel–floodplain complex. Thus, η denotes channel bed–floodplain averaged (mean) elevation. Summing over all grain sizes, the following standard Exner equation describing bed elevation evolution is obtained:

$$(1 - \lambda_p) \frac{\partial \eta}{\partial t} = - \frac{(1 + \Lambda) \Omega I_f B_{bf}}{B_f} \frac{\partial q_T}{\partial x} \quad (19)$$

Between Eqs (18) and (19), the following equation describing the evolution of the GSD of the active layer is obtained:

$$(1 - \lambda_p) \left[L_a \frac{\partial F_i}{\partial t} + (F_i - F_{li}) \frac{\partial L_a}{\partial t} \right] = - \frac{(1 + \Lambda) \Omega I_f B_{bf}}{B_f} \left(\frac{\partial(q_T f_i)}{\partial x} - F_{li} \frac{\partial q_T}{\partial x} \right) \quad (20)$$

Active layer thickness and stratigraphy

Active layer thickness L_a is assumed to scale with dune height Δ_{dune} in the case of sand-bed rivers (Deigaard, 1980). Although the presence or absence of dunes in the Yellow River remains somewhat poorly understood (Ma et al., 2017; Parker, Fu, Zhang, Zinger, & Konsoer, 2013) we employ a relation by Julien and Klaasen (1995) to estimate the dune height Δ_{dune} in this study. Julien and Klaasen (1995) described dune height as a function of flow depth H and median grain size D_{50} of the bed

surface in the following form:

$$\Delta_{dune} = \xi H \left(\frac{D_{50}}{H} \right)^{0.3} \quad (21)$$

where ξ denotes a constant that varies between 0.8 and 8. In implementing the above formula, we have replaced D_{50} with surface geometric mean size D_g for simplicity. The active layer thickness then takes the following form:

$$L_a = \alpha_{al} \Delta_{dune} \quad (22)$$

in which α_{al} is a user-specified constant, which is the ratio of active layer thickness to dune height. Taking approximately the median value of 0.8–8, the value of ξ is set to be $\xi = 4$, and the value of α_{al} is set to be $\alpha_{al} = 2$, respectively. When the bed is subject to degradation and the GSD of the active layer is coarser than that of the substrate, the simulation is subject to ellipticity (Ribberink, 1987; Stecca, Siviglia, & Blom, 2014). The values of ξ and α_{al} have been carefully selected so as to avoid such numerical instability. The GSD of the active layer evolves as the bed aggrades or degrades. As the bed aggrades, some combination of the bed material load and the active layer material is transferred to the substrate, while as the bed degrades the material in the substrate is transferred to the active layer. Thus, the following condition holds:

$$F_{li} = \begin{cases} F_{subi} & \text{for } \frac{\partial \eta}{\partial t} < 0 \\ \alpha_{trans} F_i + (1 - \alpha_{trans}) f_i & \text{for } \frac{\partial \eta}{\partial t} > 0 \end{cases} \quad (23)$$

where F_{subi} and α_{trans} denote the volume fraction content in the substrate and the weighting factor for the substrate–active layer sediment transformation, respectively (Hoey & Ferguson, 1994; Toro-Escobar, Parker, & Paola, 1996). Wright and Parker (2005a, 2005b) argue that the value of α_{trans} should be close to 1 in the case of sand-bed rivers, because sediment in the load cannot easily be sieved through the surface layer (active layer), which becomes finer when the bed aggrades. However, they also call for the further investigation concerning this point. Thus, due to a lack of knowledge of the dynamics at the surface layer–substrate interface, the value of α_{trans} is set to be $\alpha_{trans} = 0.5$ in this study. The uncertainty associated with the selection of the value should be kept in mind.

We first allow the bed to aggrade at the scale of centuries so as to reproduce the present-day upward concave profile of the LYR, and concomitant downstream fining. We then substantially reduce the sediment supply so as to mimic the effect of Xiaolangdi dam in 2000, and model incisional degradation and bed coarsening at the decadal scale. It is thus necessary to store the vertical stratigraphy, i.e. the vertical variation of the GSD of the substrate created by aggradation in the model, so that subsequent degradation consumes this material. More specifically, the volume fraction content of the i th size range grain in the

substrate F_{subi} , which can vary in the streamwise and vertical direction as the flow emplaces new substrate during aggradation, needs to be stored. In order to achieve this, a numerical method proposed by Viparelli, Sequeiros, Cantelli, Wilcock, and Parker (2010) is implemented. At each computational node, the substrate is divided into storage sublayers, except at the top, which corresponds to the interface between the active layer and substrate (Fig. S3). Each storage sublayer has the thickness L_s , which is set to be 1 m in this study. As the bed aggrades, new storage layers are added to the top as needed, whereas as the bed degrades, the storage layers are consumed in order from the top down. More details on the implementation of stratigraphy storage are found in Viparelli et al. (2010).

Boundary conditions

The bed elevation is fixed at the downstream end; we do not consider backwater effects and delta progradation, or any external forcing such as tectonic subsidence or sea level rise. Bed material is supplied only at the upstream end, and we consider no tributaries or other sources of sediment supply within the study reach. Although the channel we consider is for the most part in a low-amplitude meandering configuration, neither channel migration nor secondary flow is considered in the 1-D calculation presented here.

6.2 Computational set-up

Computational scenario

First, we run the model for several hundred years with “pre-Xiaolangdi” conditions, for which water discharge and bed material supply are relatively high. This allows us to “spin-up” the model so as to loosely reproduce recent “pre-Xiaolangdi” conditions, including the aggressive bed aggradation and the tendency for downstream fining that was observed in 1980s (Fig. 2). It should be kept in mind that our interest herein is to reproduce the trends of downstream fining as well as bed coarsening in response to dam closure. The time required for the spin-up simulation does not have a precise physical meaning, but must be large enough to allow the river to reach an approximation of the pre-Xiaolangdi profile from the specified initial bed profile. We then change to “post-Xiaolangdi” conditions, for which the bed material supply is reduced significantly but water discharge is kept unchanged, and run for 10 more years.

Bankfull discharge and bed material feed rate

Wu et al. (2008) reported a time series of annual sediment load and bankfull discharge between 1960 and 2003 at various locations, including the Huayuankou and Lijin gauging stations. From the time series at the Huayuankou station, we selected a representative value of the annual sediment load by taking an average between 1980 and 1999. We assumed, based on an analysis of the GSD of the suspended load at Huayuankou, that 55% of annual sediment load is bed material and the remaining

45% is wash load. Here wash load corresponds to material finer than $15\ \mu\text{m}$ (Ma et al., 2017). Thus, for the “pre-Xiaolangdi” condition, the bed material feed rate $G_{Tfeed,pre}$ is set to be $G_{Tfeed,pre} = 385\ \text{Mt yr}^{-1}$ ($700\ \text{Mt yr}^{-1}$ including wash load. A similar number is reported by Gao et al., 2010; Wang et al., 2007).

In a similar manner, bankfull discharge for the “pre-Xiaolangdi” condition was determined by taking the average of the time series between 1980 and 1999 at Lijin station reported by Wu et al. (2008). We selected $4500\ \text{m}^3\ \text{s}^{-1}$ as the representative bankfull discharge of the reach ($Q_{bf} = 4500\ \text{m}^3\ \text{s}^{-1}$; a similar value is reported by Wang & Li, 2011).

The annual sediment load averaged between 2000 and 2003 in the report by Wu et al. (2008) shows that it has decreased by nearly 90% compared to the “pre-Xiaolangdi” condition. For the “post-Xiaolangdi” condition, therefore, we reduce the annual sediment supply rate by a factor of 1/10 (i.e. $G_{Tfeed,post} = 38.5\ \text{Mt yr}^{-1}$, excluding wash load). Meanwhile, bankfull discharge is left unchanged for simplicity.

Model geometry and planform

The computational setup is summarized in Table S1 in the online supplemental data. The modelling reach is between Xiaolangdi Dam and the river mouth, which is about 860 km ($L = 860\ \text{km}$, where L is the reach length). Although there are some upstream sections where the channel is braided, here we assume that the channel is single-thread, rectangular and sinuous everywhere (Fig. S2a), in light of the fact that 87% of the study reach is indeed single-channel. Reach-representative bankfull channel width B_{bf} is set to 500 m ($B_{bf} = 500\ \text{m}$) and is fixed in space and time for both “pre-Xiaolangdi” and “post-Xiaolangdi” conditions.

The active floodplain width, within which overbank deposition of wash load occurs, is for both the “pre-Xiaolangdi” and “post-Xiaolangdi” conditions selected based on the river cross-section reported in He et al. (2012). For the “pre-Xiaolangdi” period, the active floodplain width $B_{f,pre}$ is set to be the constant value 13,000 m, which corresponds to the distance between the “primary levees” (Fig. S2b). Meanwhile the active floodplain width for the “post-Xiaolangdi” condition $B_{f,post}$ is set to be equal to 2500 m, which corresponds to the distance between the “farming levees” (Fig. S2b) (assuming that only the floodplain within the farming levees is active). The latter assumption is justified by the fact that ever since the installation of Xiaolangdi Dam the flood discharge has been carefully controlled, and thus the flow does not escape the farming levees.

Initial condition

Initial down-channel slope S_l is purposely set to be relatively low so that the “spin-up” simulation under “pre-Xiaolangdi” conditions results in long-term bed aggradation and downstream fining toward a state similar to that just before the closure of Xiaolangdi Dam. Thus, the initial channel slope is set to be

$S_f = 0.00005$ everywhere. As one of the initial conditions, the GSD of the bed surface is set everywhere to be identical to the substrate GSD. For this purpose, we use the modern GSD of the bed material at Lijin station. The GSD of the sediment feed is taken to be identical to that of the total bed material load at Huayuankou gauging station, as determined from the YRIHR dataset mentioned above. The GSDs of initial bed surface, substrate, and bed material supplied at the upstream end are shown in Fig. 8f. Note that while the GSDs of the bed surface and substrate vary over time and space, the GSD of the bed material supply does not.

Auxiliary parameters

The Chezy friction coefficient (C_z) is determined based on an analysis of the YRIHR dataset for the Lijin, Sunkou, and Gao-cun gauging stations; a characteristic value is found to vary between approximately 10 and 80. We select the characteristic value $C_z = 30$ (Fig. S4 in the online supplemental data) for use. Bed porosity (λ_p) and channel sinuosity Ω are set to 0.3 and 1.3, respectively. The flood intermittency factor (I_f) is determined in such a way that our proposed sediment transport relation

would produce the same mean annual bed material load as that observed based on the YRIHR database for “pre-Xiaolangdi” conditions, using the given hydraulic conditions and initial conditions. By means of the values $Q_{bf} = 4500 \text{ m}^3 \text{ s}^{-1}$ and $G_{Tfeed,pre}$ (bed material feed rate for the “pre-Xiaolangdi” condition) = 385 Mt yr^{-1} , we determine that $I_f = 0.13$. This is used for both “pre-Xiaolangdi” and “post-Xiaolangdi” conditions.

6.3 Results

In the first 600 years of the “spin-up” run under the “pre-Xiaolangdi” condition, the bed aggrades everywhere due to the high bed material feed rate, except at the downstream end where the bed elevation is fixed (Fig. 8a). The degree of aggradation is greater along the upstream reach than the downstream reach, resulting in an upward-concave bed profile, in which channel slope decreases downstream (Fig. 8a and 8b). At 600 years, the model predicts a pattern of downstream fining of geometric mean grain size of the bed surface D_g that adequately reflects the observed pattern (YRIHR dataset in Fig. 8c). Figure 8f shows the GSDs of bed material feed (from field data at Huayuankou),

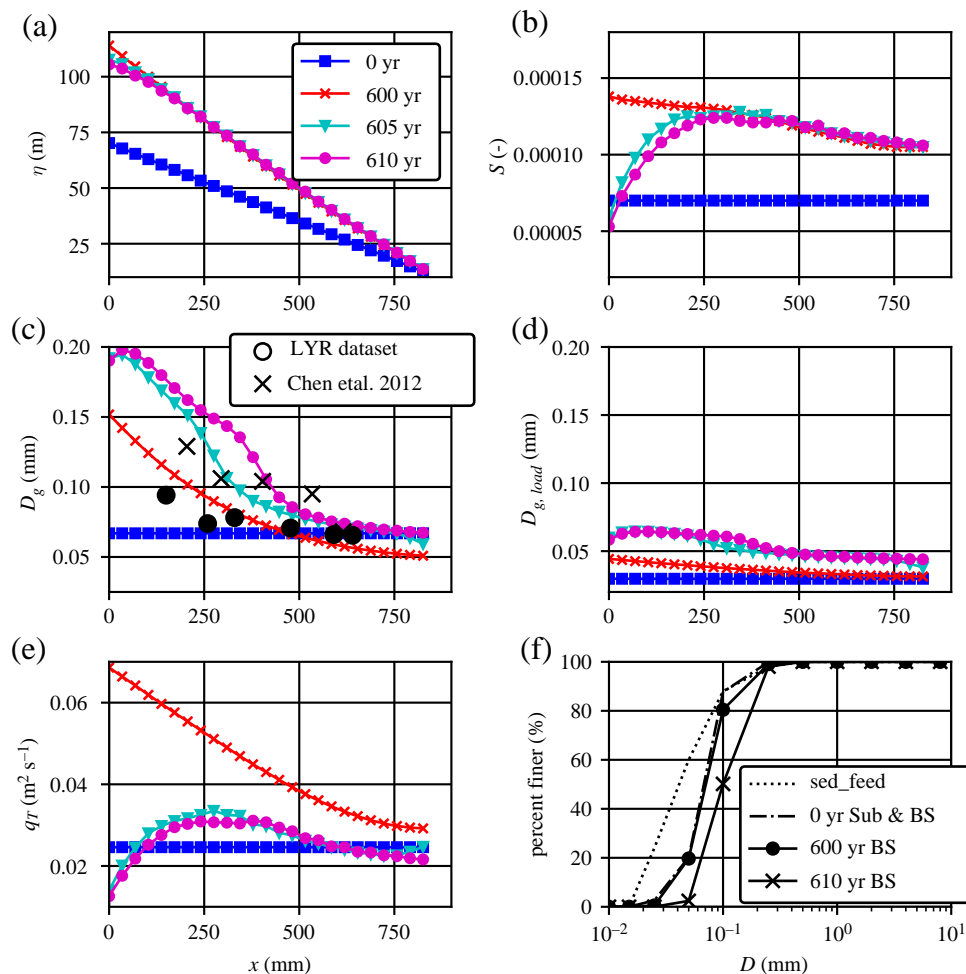


Figure 8 Computational results for “pre-Xiaolangdi” condition followed by “post-Xiaolangdi” condition. (a) Bed elevation (channel-floodplain average); (b) downstream channel slope; (c) geometric mean size of bed surface material; (d) geometric mean size of total load; (e) volume bed material transport rate per unit width. Also (f) shows GSD of feed material (dashed line), substrate and initial bed surface (broken line), and bed surface at time 600 years and 610 years, at the middle of the reach (430 km from upstream end). The legend in Fig. 8a also applies to Fig. 8b–e

initial substrate (which is identical to the initial bed surface, based on field data at Lijin), and the bed surface at the midpoint of our study reach (430 km from the upstream) at 600 years (as computed from the model).

When the bed material supply is reduced at 600 years (“post-Xiaolangdi” condition), the upstream part of the reach starts degrading substantially, whereas the downstream part of the reach remains unchanged after 10 years (610 years total, Fig. 8a). The decrease in bed material supply also leads to bed surface coarsening (armouring) (Fig. 8c). While the total bed material load per unit width decreases as a result of bed material supply reduction (Fig. 8e), the geometric mean grain size of total load $D_{g,load}$ becomes coarser (Fig. 8d and 8e). It should be noted that the transported material (total bed material load) is always finer than bed surface (Fig. 8c and 8d). By 10 years after the sediment supply reduction (610 years in total), the model generally predicts the observed trend of temporal bed coarsening, as well as the observed overall trend the downstream fining (Fig. 8c) in response to the bed supply reduction, in agreement with the findings of Chen et al. (2012) and Ta et al. (2011). Figure 8f shows the feed size distribution (as measured at Huayuankou), the bed surface size distribution at 600 years at 430 km below the upstream end (as predicted by the spin-up run), and the predicted bed surface size distribution at 610 years (10 years after cutting off the sediment supply). The coarsening of the bed surface in a decade is readily apparent.

7 Discussion

7.1 Cause of downstream fining and bed coarsening in the LYR

At 600 years in the model results, the bed profile exhibits an upward-concave shape due to aggressive bed aggradation toward the upstream end of the reach (Fig. 8a and 8b). This results in a downstream decrease in bed shear stress, and ultimately results in size-selective transport, which is a common feature in sand-bed rivers and gravel-bed rivers (Hoey & Ferguson, 1994; Wright & Parker, 2005a, 2005b). This can be seen in Fig. 8d, where a pattern of downstream decrease in the geometric mean grain size of the total load $D_{g,load}$ is illustrated.

When the sediment supply is reduced, the upstream section of the reach starts degrading, leading to a downward-convex profile in the upper half of the section (Fig. 8a and 8b). The bed surface becomes coarser everywhere as a consequence of sediment supply reduction. This coarsening represents a classic case of the bed armouring more commonly seen in gravel-bed rivers (e.g. Parker, Hassan, & Wilcock, 2007); since coarser materials are more difficult to be transported by flow, relatively coarser material remains on the bed surface, creating a bed surface that is coarser than the substrate. The degree of bed coarsening is strongest toward the upstream end of the domain, where bed degradation is substantial (Fig. 8a). This acts to strengthen the pattern of downstream fining after sediment supply reduction.

It should be kept in mind, however, that the substrate also becomes coarser toward the upstream end of the reach during the first 600 years of the “spin-up” run. This can be inferred by the fact that the bed surface, which was gradually buried into the substrate, becomes coarser in the upstream half of the reach. When the bed material supply rate is reduced, this coarsened substrate comes to the surface due to bed degradation, and this enhances the bed surface coarsening at the upstream reach. In other words, downstream fining after sediment supply reduction is likely caused by (i) size-selective transport and (ii) coarsening of substrate during the “spin-up” simulation toward the upstream end of the domain, which is mined during later degradation.

The predicted pattern of downstream fining reasonably closely tracks observed values, but does not precisely match them in either the “pre-Xiaolangdi” condition or the “post-Xiaolangdi” condition (Fig. 8c). We emphasize that our implementation is “broad-brush”, excluding many details of the highly leveed and managed LYR. The consideration of such factors as spatial variation in channel and levee widths, water discharge hydrographs including the effect of water extraction, delta propagation, variation in flood intermittency, and any tectonic activity would give more precision to the model. The implementation of such factors is tedious but straightforward.

The trend of downstream fining and coarsening can also be seen in the total bed material load; at 600 years, $D_{g,load}$ exhibits a decline in the downstream direction. Although Fig. 7 suggests that $D_{g,load}$ should increase with decreasing bed shear stress, downstream fining of the bed surface suppresses the effect of streamwise decline in the shear stress. When the bed material supply is decreased, overall bed slope declines (hence bed shear stress declines), thus total load becomes coarser accordingly. Meanwhile the trend of downstream fining of the load is maintained due to the strong trend of downstream fining of the bed surface.

7.2 Model applicability to the sorting problem in sand-silt-bed rivers

The proposed relation for the prediction of bed material load for mixtures is a surface-based relation rather than substrate-based relation. In addition to various merits in utilizing a surface-based relation, which are well summarized in Wilcock and Crowe (2003), there is an advantage in terms of data availability. Specifically, GSD data for the bed surface tends to be much more readily available than data for the substrate. The fact that the relation contains no critical Shields number for incipient motion of sediment not only corresponds to the reality of typical sediment transport events in the LYR, which are far above the threshold of motion, but also makes the form of the proposed relation simpler, hence more user-friendly. Note that (a) the proposed model is an extended form of the EH total load relation, which also does not incorporate a critical bed shear stress, and (b) in the case of sand-silt-bed rivers, the bed material is so fine

that most of the sediment is in motion even during low flow. In spite of the simplicity of the proposed model, it is capable of dealing with the sorting phenomena of downstream fining and armouring as they occur in the sand-silt bed LYR.

8 Conclusions

Grain sorting such as downstream fining and bed surface coarsening is not unique to sand-bed rivers or gravel-bed rivers; we have found that silt-rich rivers such as the LYR exhibit grain sorting. In order to treat grain sorting of fine material, we developed a total bed material relation for fine sediment mixtures. We utilized the general form of Engelund and Hansen total load relation (1967), which is commonly used as a predictor of total load for sand-bed rivers but is invalid for sand-silt-bed rivers, to develop our relation. In order to quantify our proposed relation, a database including bed surface GSD is required.

We have evaluated our relation for the case of the LYR using field data collected at the Lijin gauging station. We find that the transport of coarser grains tends to have less dependency on hydraulic conditions than that of finer grains, and that as the flow intensity increases, the bed material load becomes ever finer compared to that of the bed surface. This is in contrast to the case of gravel-bed rivers, whereby the GSD of the total load approaches that of the bed surface with increasing bed shear stress. A relation for suspended load of mixtures in sand-bed rivers, however, predicts a load that is finer than the bed surface over a wide range (Wright & Parker, 2004).

Our proposed relation is capable of reproducing ongoing downstream fining and bed coarsening due to bed material supply reduction in the LYR. Downstream fining due to selective transport is reproduced as a consequence of historic aggressive bed aggradation associated with an upward-concave river bed profile, both of which are responses to massive sediment supply from the Loess Plateau. Bed coarsening (armouring) is reproduced in accordance with bed degradation due to substantially reduced bed material supply rate at the upstream end of the modelled reach, which is in turn due to sediment retention in the recently closed Xiaolangdi Dam.

Although our proposed model of grain size specific sediment transport likely requires some site-specific calibration, the form of the equation is relatively simple, in part due to the absence of a critical Shields number for incipient motion of sediment. Moreover, with appropriate calibration, it can easily be applied to grain sorting problems in other fine-grained rivers with sand-silt-beds such as the Pilcomayo River at the border of Argentina and Paraguay (Martín-Vide et al., 2014).

Acknowledgements

We very gratefully acknowledge the students in Parker's course, "River Morphodynamics" in the spring of 2015 for their help with data extraction, organization and analysis: C-G An, D.S.

Ancalle Reyes, Z.D. Barnaal, Q-T Gao, J. Geldmeyer, A.M. Hamed, T-Y He, E. Lacunza, F.P. Maciel Yo, M.J. Reed, F.A. Neira Ruiz, J.E. San Juan Blanco, R.H. Takahashi, D-C Wang, H. Wu, R-J Zeng and R-S. Zhou.

Funding

Kensuke Naito, Hongbo Ma, Jeffrey Nittrouer and Gary Parker gratefully acknowledge the National Science Foundation [EAR grants 1427262; 1209402]. Yuanfeng Zhang acknowledges the National Natural Science Foundation of China [grant 51379087]. Yuanjian Wang also acknowledges support from the National Nature Science Foundation of China [grants 51509102; 51679104; 5153000441]; Division of Earth Sciences.

Supplemental data

Supplemental data for this article can be accessed [doi:10.1080/00221686.2018.1555554](https://doi.org/10.1080/00221686.2018.1555554).

Notation

A, B	= coefficient and exponent in the general form of the Engelund–Hansen sediment transport relation (–)
A_i, B_i	= coefficient and exponent in the proposed sediment transport relation for the i th size range grain (–)
B_{bf}	= reach-representative bankfull channel width (m)
B_f	= floodplain width (m)
C_f	= bed friction coefficient (–)
C_z	= dimensionless Chezy resistance coefficient (–)
D_{50}	= median grain size of bed surface (mm)
D_g	= geometric mean grain size of bed surface (mm)
$D_{g,load}$	= geometric mean grain size of total bed material load (mm)
D_i	= grain size of i th size range (mm)
f_i	= volume fraction content of bed material within grain size interval i (–)
F_i	= volume fraction content of bed material in bed surface (active layer) within grain size interval i (–)
F_{li}	= volume fraction content of bed material at the interface between bed surface and substrate within grain size interval i (–)
F_{subi}	= volume fraction content of bed material in substrate within grain size interval i (–)
g	= gravitational acceleration (m s^{-2})
$G_{T,feed}$	= mass rate of bed material supply at the upstream end of the reach (t yr^{-1})
H	= flow depth (m)
H_{bf}	= bankfull depth (m)
I_f	= flood intermittency (–)
L	= reach length (km)
L_a	= active layer thickness (m)

L_s	= substrate storage layer thickness (m)
N	= number of bins in the grain size distribution of the proposed sediment transport relation (–)
N_T^*	= proposed dimensionless form of total bed material load (–)
N_i^*	= proposed dimensionless form of bed material load of sediment within grain size interval i (–)
q_i	= volume total bed material load per unit width within grain size interval i ($\text{m}^2 \text{s}^{-1}$)
q_T	= volume total bed material load per unit width ($\text{m}^2 \text{s}^{-1}$)
q_T^*	= dimensionless form of volume total bed material load per unit width (–)
Q_{bf}	= representative bankfull discharge ($\text{m}^3 \text{s}^{-1}$)
R	= submerged specific gravity of sediment (–)
S	= down-channel slope (–)
t	= time (s)
U	= depth-averaged velocity (m s^{-1})
u_*	= shear velocity (m s^{-1})
x	= streamwise coordinate (m)
α_{al}	= ratio of active layer thickness to dune height (Eq. (20)) (–)
α_{trans}	= weight factor for the substrate-active layer sediment exchange fractions (Eq. (21)) (–)
Δ_{dune}	= dune height (m)
η	= channel bed-floodplain averaged elevation (m)
Λ	= ratio of volume wash load deposition on the floodplain to volume deposition of bed material in the channel (–)
λ_p	= bed porosity (–)
ξ	= constant in the dune height relation (Eq. (19)) (–)
ρ	= density of the water-sediment mixture (kg m^{-3})
τ_b	= bed shear stress (Pa)
τ_g^*	= dimensionless bed shear stress for the geometric mean bed surface material size (–)
τ_i^*	= dimensionless bed shear stress for the sediment within grain size interval i (–)
Ω	= channel sinuosity (–)

ORCID

Kensuke Naito  <http://orcid.org/0000-0001-8683-0846>

References

- Allan, J. D., & Castillo, M. M. (2007). *Stream ecology: Structure and function of running waters*. New York, NY: Springer.
- Ashida, K., & Michiue, M. (1972). Study on hydraulic resistance and bed-load transport rate in alluvial streams. In *Proceedings of the Japan society of civil engineers* (Vol. 1972, No. 206, pp. 59–69). Japan Society of Civil Engineers (in Japanese).
- Bettess, R. (1994). Sediment transport and channel stability. In P. P. Calow & G. E. Petts (Eds.), *The rivers handbook: Hydrological and ecological principles* (Vol. 2, pp. 227–253). Oxford: Blackwell Science.
- Blom, A., Arkesteijn, L., Chavarrias, V., & Viparelli, E. (2017). The equilibrium alluvial river under variable flow and its channel-forming discharge. *Journal of Geophysical Research: Earth Surface*, 122(10), 1924–1948.
- Blom, A., Viparelli, E., & Chavarrias, V. (2016). The graded alluvial river: Profile concavity and downstream fining. *Geophysical Research Letters*, 43(12), 6285–6293.
- Brownlie, W. R. (1981). *Prediction of flow depth and sediment discharge in open channels* (Report No. KH-R-43A). Pasadena, California, USA: W. M. Keck Laboratory of Hydraulics and Water Resources, California Institute of Technology, 232.
- Chen, J., Zhou, W., & Qiang, C. (2012). Reservoir sedimentation and transformation of morphology in the lower yellow river during 10 year's initial operation of the Xiaolangdi reservoir. *Journal of Hydrodynamics, Ser. B*, 24(6), 914–924.
- Chen, Y., Wang, K., Lin, Y., Shi, W., Song, Y., & He, X. (2015). Balancing green and grain trade. *Nature Geoscience*, 8(10), 739–741.
- Cohn, T. A. (1995). Recent advances in statistical methods for the estimation of sediment and nutrient transport in rivers. *Reviews of Geophysics*, 33(S2), 1117–1123.
- Deigaard, R. (1980). *Longitudinal and transverse sorting of grain sizes in alluvial rivers* (Paper No. 26). Institute of Hydrodynamics and Hydraulic Engineering, Technical University of Denmark.
- Engelund, F., & Hansen, E. (1967). *A monograph on sediment transport in alluvial streams*. Copenhagen K: Technical University of Denmark Ostervoldgade 10.
- Frings, R. M. (2008). Downstream fining in large sand-bed rivers. *Earth-Science Reviews*, 87(1–2), 39–60.
- Gao, P., Zhang, X., Mu, X., Wang, F., Li, R., & Zhang, X. (2010). Trend and change-point analyses of streamflow and sediment discharge in the Yellow River during 1950–2005. *Hydrological Sciences Journal–Journal des Sciences Hydrologiques*, 55(2), 275–285.
- He, L., Duan, J., Wang, G., & Fu, X. (2012). Numerical Simulation of Unsteady Hyperconcentrated Sediment-Laden Flow in the Yellow River. *Journal of Hydraulic Engineering*, 138(11), 958–969.
- Hicks, D. M., & Gomez, B. (2016). Sediment transport. In G. M. Kondolf & H. Piégay (Eds.), *Tools in fluvial geomorphology* (pp. 324–356). Chichester, UK: John Wiley & Sons Ltd.
- Hirano, M. (1971). River-bed degradation with armoring. In *Proceedings of the Japan society of civil engineers* (Vol. 1971, No. 195, pp. 55–65). Japan Society of Civil Engineers (in Japanese).
- Hoey, T. B., & Ferguson, R. I. (1994). Numerical simulation of downstream fining by selective transport in gravel bed rivers: Model development and illustration. *Water Resources Research*, 30(7), 2251–2260.

- Hunziker, R., & Jaeggi, M. N. R. (2002). Grain sorting processes. *Journal of Hydraulic Engineering*, 128(12), 1060–1068.
- Jiongxin, X. (1999). Erosion caused by hyperconcentrated flow on the Loess Plateau of China. *Catena* 36(1–2), 1–19.
- Julien, P. Y., & Klaasen, G. J. (1995). Sand-dune geometry of large rivers during floods. *Journal of Hydraulic Engineering*, 121(9), 657–663.
- Kuhnle, R. A. (1992). Fractional transport rates of bedload on Goodwin Creek. In Billi, P., Hey, R. D., Thorne, C. R., & Tacconi, P. (Eds.), *Dynamics of gravel-bed rivers* (pp. 141–155). Chichester: John Wiley & Sons.
- Long, Y., & Zhang, Y. (2002). Study on the Yellow River sediment from the viewpoint of total sediment. *Yellow River*, 24(8), 28–29. (in Chinese).
- Ma, H., Nittrouer, J. A., Naito, K., Fu, X., Zhang, Y., Moodie, A. J., . . . Parker, G. (2017). The exceptional sediment load of fine-grained dispersal systems: Example of the Yellow River, China. *Science Advances* 3(5), e1603114.
- MacArthur, R. C., Neill, C. R., Hall, B. R., Galay, V. J., & Shvidchenko, A. B. (2008). Overview of sedimentation engineering. In M. H. Garcia (Ed.), *Sedimentation engineering: Processes, measurements, modeling, and practice* (pp. 1–20). Reston, VA: American Society of Civil Engineers.
- Martín-Vide, J. P., Amarilla, M., & Zárata, F. J. (2014). Collapse of the Pilcomayo River. *Geomorphology*, 205, 155–163.
- Milliman, J. D., & Meade, R. H. (1983). World-wide delivery of river sediment to the oceans. *The Journal of Geology*, 91(1), 1–21.
- Paola, C., Heller, P. L., & Angevine, C. L. (1992). The large-scale dynamics of grain-size variation in alluvial basins, 1: Theory. *Basin Research*, 4(2), 73–90.
- Parker, G. (1990). Surface-based bedload transport relation for gravel rivers. *Journal of Hydraulic Research*, 28(4), 417–436.
- Parker, G. (1991a). Selective sorting and abrasion of river gravel. I: Theory. *Journal of Hydraulic Engineering*, 117(2), 131–147.
- Parker, G. (1991b). Selective sorting and abrasion of river gravel. II: Applications. *Journal of Hydraulic Engineering*, 117(2), 150–171.
- Parker, G. (2008). Transport of gravel and sediment mixtures. In M. H. Garcia (Ed.), *Sedimentation engineering: Processes, measurements, modeling, and practice* (pp. 165–251). Reston, Virginia: American Society of Civil Engineers.
- Parker, G., Fu, X., Zhang, Y., Zinger, J., & Konsoer, K. (2013, September). Bedform regime diagram for rivers and turbidity currents: Conditions for the formation and obliteration of dunes. In Z. Wang (Ed.), *Proceedings of the 2013 international association for hydro-environment engineering and research congress* (pp. 8–13). Chengdu, China: IAHR.
- Parker, G., Hassan, M., & Wilcock, P. R. (2007). Adjustment of the bed surface size distribution of gravel-bed rivers in response to cycled hydrographs. In H. Habersack, H. Piégay, & M. Rinaldi (Eds.), *Gravel-bed rivers VI: From process understanding to river restoration* (pp. 241–285). New York, NY: Elsevier Science & Technology.
- Parker, G., & Klingeman, P. C. (1982). On why gravel bed streams are paved. *Water Resources Research*, 18(5), 1409–1423.
- Pierson, T. C. (2005). Hyperconcentrated flow—Transitional process between water flow and debris flow. In M. Jakob, O. Hungr, & D. M. Jakob (Eds.), *Debris-flow hazards and related phenomena* (pp. 159–202). Berlin, Germany: Springer.
- Ribberink, J. S. (1987). *Mathematical modelling of one-dimensional morphological changes in rivers with non-uniform sediment* (Doctoral dissertation). Delft University of Technology, Delft, The Netherlands.
- Stecca, G., Siviglia, A., & Blom, A. (2014). Mathematical analysis of the Saint-Venant-Hirano model for mixed-sediment morphodynamics. *Water Resources Research*, 50, 7563–7589. doi:10.1002/2014WR015251
- Ta, W., Wang, H., & Jia, X. (2011). Downstream fining in contrasting reaches of the sand-bedded Yellow River. *Hydrological Processes*, 25(24), 3693–3700.
- Tian, S., Wang, Z., Li, Z., & Li, Y. (2016). Effects of soil property of loess plateau on sediment characteristics in the yellow river. *International Journal of Sediment Research*, 5, 74–80.
- Toro-Escobar, C. M., Parker, G., & Paola, C. (1996). Transfer function for the deposition of poorly sorted gravel in response to streambed aggradation. *Journal of Hydraulic Research*, 34(1), 35–53.
- Tsujimoto, T. (1991). *Mechanics of sediment transport of graded materials and fluvial sorting* (Report No. 0155041). Kanazawa, Japan: Kanazawa University.
- Viparelli, E., Sequeiros, O. E., Cantelli, A., Wilcock, P. R., & Parker, G. (2010). River morphodynamics with creation/consumption of grain size stratigraphy 2: Numerical model. *Journal of Hydraulic Research*, 48(6), 727–741.
- Wang, H., Bi, N., Saito, Y., Wang, Y., Sun, X., Zhang, J., & Yang, Z. (2010). Recent changes in sediment delivery by the Huanghe (Yellow River) to the sea: Causes and environmental implications in its estuary. *Journal of Hydrology*, 391(3–4), 302–313.
- Wang, H., Yang, Z., Saito, Y., Liu, J. P., Sun, X., & Wang, Y. (2007). Stepwise decreases of the Huanghe (Yellow River) sediment load (1950–2005): Impacts of climate change and human activities. *Global and Planetary Change*, 57(3–4), 331–354.
- Wang, S., Fu, B., Piao, S., Lü, Y., Ciais, P., Feng, X., & Wang, Y. (2016). Reduced sediment transport in the Yellow River due to anthropogenic changes. *Nature Geoscience*, 9(1), 38–41.
- Wang, S., & Li, Y. (2011). Channel variations of the different channel pattern reaches in the lower Yellow River from 1950 to 1999. *Quaternary International*, 244(2), 238–247.
- Wang, Z., Wang, W., & Tian, S. (2007). Mineral composition and distribution of the sediment in the Yellow

- River basin. *International Journal of Sediment Research*, 5, 1–8.
- Wilcock, P. R. (1997). The components of fractional transport rate. *Water Resources Research*, 33(1), 247–258.
- Wilcock, P. R., & Crowe, J. C. (2003). Surface-based transport model for mixed-size sediment. *Journal of Hydraulic Engineering*, 129(2), 120–128.
- Woo, H. S., Julien, P. Y., & Richardson, E. V. (1986). Washload and fine sediment load. *Journal of Hydraulic Engineering*, 112(6), 541–545.
- Wright, L. D., Wiseman, W. J. Jr., Tang, Z.-S., Bornhold, B. D., Keller, G. H., Prior, D. B., & Suhayda, J. N. (1990). *Continental Shelf Research*, 10(1), 1–40.
- Wright, S., & Parker, G. (2004). Flow resistance and suspended load in sand-bed rivers: Simplified stratification model. *Journal of Hydraulic Engineering*, 130(8), 796–805.
- Wright, S., & Parker, G. (2005a). Modeling downstream fining in sand-bed rivers. I: Formulation. *Journal of Hydraulic Research*, 43(6), 612–619.
- Wright, S., & Parker, G. (2005b). Modeling downstream fining in sand-bed rivers II: Application. *Journal of Hydraulic Research*, 43(6), 620–630.
- Wu, B., & Long, Y. (1993). Several modifications for sediment transport capacity formulas of the Yellow River. *Yellow River*, 95(7), 1–4. (in Chinese).
- Wu, B., van Maren, D. S., & Li, L. (2008). Predictability of sediment transport in the Yellow River using selected transport formulas. *International Journal of Sediment Research*, 23(4), 283–298.
- Wu, B., Wang, G., Xia, J., Fu, X., & Zhang, Y. (2008). Response of bankfull discharge to discharge and sediment load in the Lower Yellow River. *Geomorphology*, 100(3–4), 366–376.
- Xue, C. (1993). Historical changes in the Yellow River delta, China. *Marine Geology*, 113(3–4), 321–330.
- Yang, C. T., Molinas, A., & Wu, B. (1996). Sediment transport in the Yellow River. *Journal of Hydraulic Engineering*, 122(5), 237–244.
- Yu, Y., Shi, X., Wang, H., Yue, C., Chen, S., Liu, Y., . . . Qiao, S. (2013). Effects of dams on water and sediment delivery to the sea by the Huanghe (Yellow River): The special role of Water-Sediment Modulation. *Anthropocene*, 3, 72–82.
- Yu, Y., Wang, H., Shi, X., Ran, X., Cui, T., Qiao, S., & Liu, Y. (2013). New discharge regime of the Huanghe (Yellow River): Causes and implications. *Continental Shelf Research*, 69, 62–72.
- Zhang, H. W., Huang, Y. D., & Zhao, L. J. (2001). A mathematical model for unsteady sediment transport in the Lower Yellow River. *Journal of Sedimentation Research*, 16(2), 150–158. (in Chinese).
- Zhang, R. (1959). A study of the sediment transport capacity of the middle and lower Yangtze River. *Journal of Sediment Research*, 4(2), 54–73. (in Chinese).
- Zhang, Y., Long, Y., & Shen, G. (1998). *Adaptability of sediment transport formula to the Yellow River. Proceedings of the 7th International Symposium on River Sedimentation*, Hong Kong, WASER.